Chapter

Coulomb Potential Modulation of Atoms by Strong Light Field: Electrostatic Tunneling Ionization and Isolated Attosecond Light Pulse

Chao Wang, Yifan Kang and Yonglin Bai

Abstract

An attosecond research upsurge has been overwhelmingly rising since the establishment of novel light source—single isolated attosecond laser in extreme ultraviolet/X-ray resulted by strong field high-order harmonics generation (HHG). In this chapter, based on the electrostatic tunneling ionization from Coulomb potential modulation of atoms by strong light field, we scrutinized the intrinsic phase of high-order harmonics and analyzed qualitatively the salient dependence of two mainstream single isolated attosecond pulse generation techniques as polarization gating(PG) and amplitude gating(AG) on carrier-envelope phase (CEP) of femtosecond driving laser. The conclusion is that the optimized CEP corresponding to the highest intensity contrast between the main and sideband attosecond pulses is $\pi/2$ and 0 for polarization gating and amplitude gating, respectively. Further, an experimental implementation was given in detail to exemplify the tricks for optimum phase-matching process of HHG from the interaction of high-intensity femtosecond laser field with noble gas target. The effects of the relative location between Gaussian-shaped driving femtosecond laser field focus and the gas target source used on the HHG phase matching were studied, and the conclusion found that the expected position of gas target for optimum phase matching is always lying behind the focal point of the driving field used.

Keywords: tunneling ionization, high-order harmonics generation, single isolated attosecond pulse, carrier-envelope phase, phase matching, few-cycle femtosecond laser

1. Introduction

With the invention in general and realization of the laser in particular by Maiman in 1960, field of optics soon entered the new era of nonlinear optics. In this regime, the optical properties of materials are no longer independent of the intensity of light—as was believed for hundreds of years before—but rather change with light intensity, giving rise to a wealth of new phenomena, effects, and applications. Today, nonlinear optics has entered our everyday life in many ways and has also

been the basis for numerous new developments in spectroscopy and laser technology. Indeed, from the moment of birth of nonlinear optics, laser physics and nonlinear optics have been intimately related to each other. Within "traditional" nonlinear optics, the absolute changes of the optical properties are tiny if one follows them versus time on a timescale of a cycle of light. This simple fact is the basis of many concepts and approximations of "traditional" nonlinear optics. Over the years, however, lasers have improved in many ways, especially in terms of the accessible peak intensities and in terms of the minimum pulse duration available. These days, over 50 years after the invention of the laser, the shortest optical pulses generated are about one and a half cycles of light in duration. This comes close to the ultimate limit of a single optical cycle [1].

Thanks to the technique of chirped-pulse amplification (CPA) and the availability of CEP stabilized few-cycle laser [2], amplified laser pulses with focused peak intensities in the range of 10^{22} W/cm^2 are available in some laboratories. As a result of this, today's light intensities can lead to substantial or even to extreme changes on the timescale of light, and the range of optics research is now shifting from the stage of perturbative to extreme (or nonperturbative) nonlinear optical mechanism [3, 4]. As for the latter, one remarkable achievement is the establishment of novel light source—single isolated attosecond (1 attosecond[as] = 10^{-18} s) laser pulse in extreme ultraviolet or even X-ray electromagnetic spectrum based on strong field HHG [5–7]. Since the fundamental processes of chemistry, biology, and materials science are triggered or mediated by the motion of electrons inside or between atoms, and that the atomic-scale motion of electrons typically unfolds within tens to thousands of attoseconds, breakthroughs in light source science are now opening the door to watching and controlling these hitherto inaccessible microscopic dynamics, opening up a new horizon of science by observing, controlling, and manipulating nature in a new dimension. Consequently, an attosecond research upsurge is overwhelmingly rising from physics, chemistry, and material science to even information processing and other fields [8–10]. What is worth mentioning is that transnational or transregional attosecond science research infrastructures are emerging, such as Extreme Light Infrastructure Attosecond Light Pulse Source (ELI-ALPS) in Szeged, Hungary. Its main objective is to establish a unique attosecond laser facility which provides developers and users with light sources within the THz to X-ray frequency range in the form of ultrashort pulses at high repetition rate.

Until now, the HHG based on the interaction between high-intensity few-cycle femtosecond laser and noble gases is regarded as the main process for generating attosecond laser pulse. The physical process in essence is frequency up-conversion resulted by optical field caused by atomic tunneling ionization, which means that, no matter what kind of single isolated attosecond pulse generation technique, such as amplitude gating [11] or polarization gating [12], the phase matching involved is the key issue, which affects the macroscopic response of the multiatom gas system and eventually determines the conversion efficiency. According to the three-step scenario of HHG proposed by Corkum [13], phase matching in process of HHG is microcosmically influenced by multiple factors involved: fundamental driving laser field, the gas system used, the high-order harmonics field that generated, and the plasma formed by the atomic ionization. It is very difficult and even impossible to carry out such a complete and accurate analysis on phase matching of HHG. So far, most theoretical analysis are addressing incompletely on one or two factors mentioned above, while the experimental demonstrations are just concerned about high-order harmonics yield, omitting intentionally or unintentionally the important details of phase matching optimization [14, 15]. Consequently, the experimental details to optimize HHG attosecond laser pulse generation are still not made clear.

In this chapter, based on the three-step scenario of HHG, we scrutinized the intrinsic phase of high-order harmonics from the atom tunneling ionization induced by strong laser field and analyzed qualitatively the salient dependence of two fundamental single attosecond pulse generation techniques as polarization gating and amplitude gating on CEP of femtosecond driving laser. Finally, an experimental implementation was given in great detail to show the way to realize optimum HHG phase matching during interaction of strong optical field with noble gas target.

2. Strong field tunneling ionization and HHG

The light intensities necessary to rapidly ionize an atom are on the order of $I \approx 10^{14} \sim 10^{16}$ W/cm^2, which is well within the nonrelativistic regime. Thus, we can ignore the laser magnetic field for the moment and focus on the laser electric field [3]. **Figure 1** visualizes this kind of ionization by high-intensity few-cycle femtosecond laser pulse for an electron bound in the Coulomb potential of a nucleus (assumed to be much more massive or fixed in space). The Gaussian linearly polarized laser pulse of $t_{FWHM} = 5\,fs$ is characterized by its electric field $E(t) = \tilde{E}(t)\,cos\,(\omega_0 t)$ with carrier photon energy $\hbar\omega_0 = 1.5\,eV$, together with the two-dimensional scheme of the resulting electric potential experienced by an electron initially bound in an atom at three characteristic points in time. The large "tilt" along the electric field vector axis in the center of the pulse can lead to tunneling of the electron out of its binding potential through the potential barrier. If the barrier height is lowered below the binding energy, above-barrier ionization can occur. For circularly polarized light, the "tilt" stays constant, but its axis rotates in time [1].

Whether we can use the concept of electrostatic tunneling for light fields oscillating depends on the ratio between the light field period and the time the electron spends within the barrier, electron tunneling time. If the tunneling time is shorter than the period of light, the laser electric field can indeed be viewed as a static field along its polarization direction that parametrically changes its instantaneous value, which is the case of HHG process-based single attosecond pulse generation. Within the "static-field approximation," the tunneling ionization rate $\Gamma_i(t)$ depends exponentially on the instantaneous barrier width $l(t)$ because the electron wave function

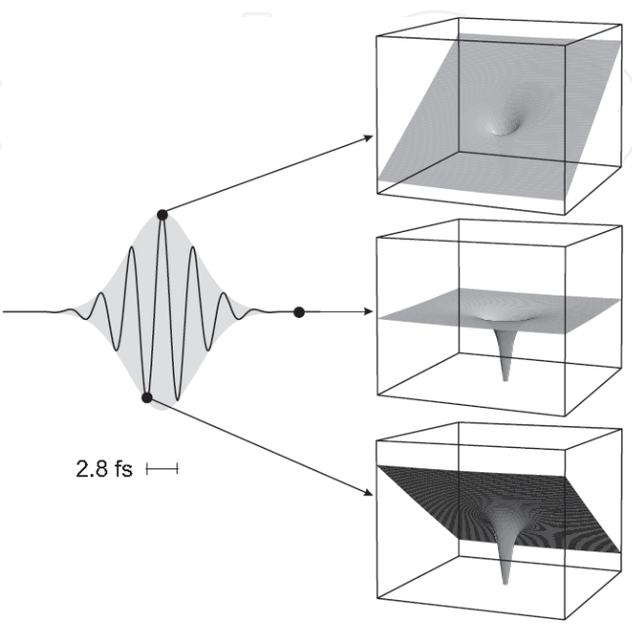

Figure 1.
Coulomb potential modulation of atoms by strong light field.

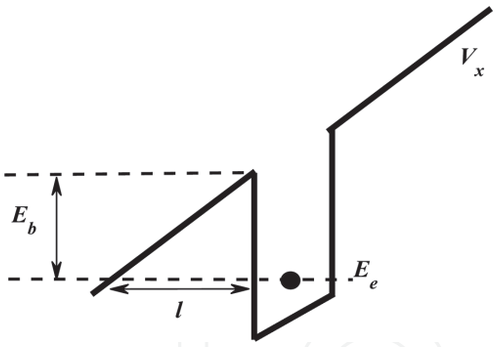

Figure 2.
Strong field-induced tunneling ionization.

is decaying exponentially in the barrier according to $\psi(x) \propto exp\,(-|k_x|x)$, as in **Figure 2**. The probability of tunneling through the barrier is $\propto |\psi(l)|^2$. Further, one can expect the general behavior $\Gamma_i(t)$ as

$$\Gamma_i(t) \propto e^{-\frac{E_b^{\frac{3}{2}}\sqrt{2m_e}}{\hbar e|E(t)|}l(t)} \tag{1}$$

Apparently, the ionization characteristics would definitely have a strong dependence on CEP of the exciting laser pulses.

To get the exact description of the HHG spectrum, one can in principle solve the time-dependent Schrödinger equation numerically for the ionization and compute the atomic dipole moment from the known instantaneous wave function $\Psi(\boldsymbol{r},t)$ via the expectation value $\langle \Psi(\boldsymbol{r},t)|-e\boldsymbol{r}|\Psi(\boldsymbol{r},t)\rangle$. Multiplying by the atoms' density delivers the macroscopic optical polarization $\boldsymbol{P}$, which is one of the main parameters in the Maxwell equations. Neglecting the propagation effects, the radiated electric field is proportional to the second temporal derivative of $\boldsymbol{P}$. The square modulus of its Fourier transform delivers the intensity spectrum of high-order harmonics. The most intuitive way to discuss semiclassically the extreme nonlinear interaction that leads to attosecond pulses is through the so-called three-step scenario introduced by Corkum [13], as in **Figure 3**. The first step (①) is the atom ionization via tunneling through the distorted Coulomb potential. Now the electron wave packet is released in the continuum where it gets accelerated by the external field (②). The third step (③) is the possible recombination with the nucleus and emission of a high-energy photon.

As for the second step, the movement of the electron wave packet can be described using Newton's second theorem of classical mechanics. Again, the magnetic field of the laser and the Coulomb potential bound on the electrons are ignored, and only the electric field of the laser is considered. And also we neglect the spatial dependence of the electric field since the wavelength of the laser field is much bigger than the distance the electron moves within the external field. We assume a laser field that the atom is exposed to is $E(t) = E_0\,cos\,(w_L t)$. The electron tunnels through the potential wall and is released into the continuum with zero velocity at position zero at birth time $t = t_i$, $v(t_i) = 0$, and $x(t_i) = 0$. When we assume that the only force experienced by the electron is $F(t) = m_e x'' = -eE(t)$, the expression for $x(t)$ follows by integrating.

$$v(t) = \frac{eE_0}{m_e w_L}\left[sin\,(w_L t) - sin\,(w_L t_i)\right], \tag{2}$$

$$x(t) = \frac{eE_0}{m_e {w_L}^2}\left[cos\,(w_L t) - cos\,(w_L t_i) + w_L(t - t_i)\sin\,(w_L t_i)\right]. \tag{3}$$

DOI: http://dx.doi.org/10.5772/intechopen.89940

Now one can use Eq. (3) to calculate the return time t_r of the electron for different tunneling times t_i. Since the process is periodic in time with a periodicity of π/w_L, we use $0 \le t_i \le 0.5T = \pi/w_L$. Using Eq. (3), one can easily get that only those electrons freed at $0 \le t_i \le 0.25T$ have the chance to return to the nucleus, as illustrated in **Figure 4**. Intuitively, the return time t_r of electron with birth time t_i is the horizontal ordinate of the intersection point formed by the laser field curve and its tangent line passing the point with $t = t_i$. And two important values for analyzing HHG are free time $\tau = t_r - t_i$ that the electron spends in the continuum and the return energy W_{kin}.

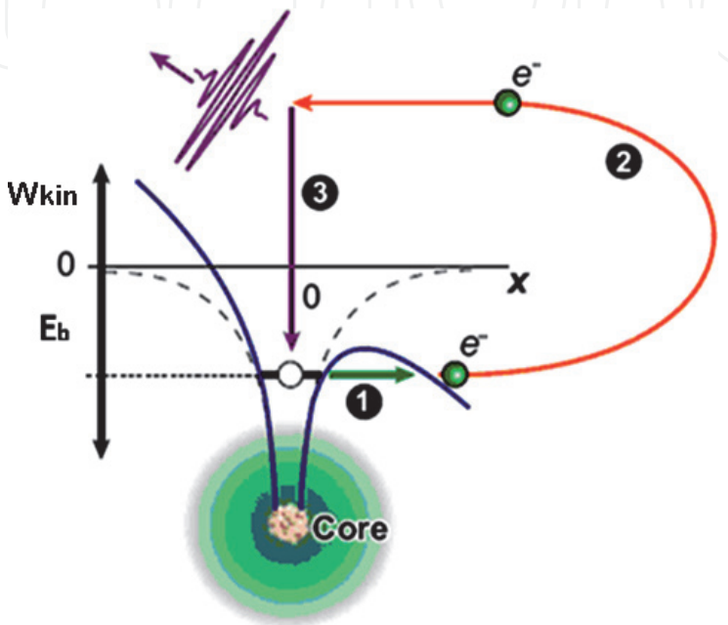

Figure 3.
Three-step scenario of high-harmonic generation.

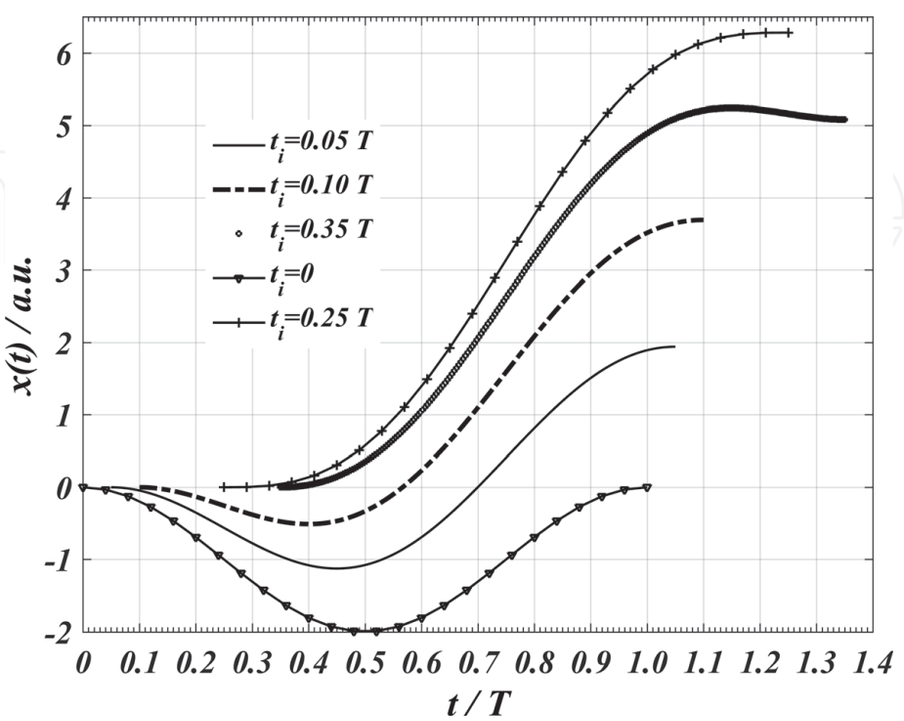

Figure 4.
Wiggling motion of electrons in external laser field.

$$W_{kin}(t_i) = 2U_p[sin\,(w_L t_r) - sin\,(w_L t_i)]^2, \tag{4}$$

$$t_i = \frac{1}{w_L} atan\left[\frac{-w_L\tau + sin\,(w_L\tau)}{1 - cos\,(w_L\tau)}\right]. \tag{5}$$

Here $U_p = e^2{E_0}^2/4m_e{w_L}^2$ is the wiggling electron's ponderomotive energy which is the period-averaged kinetic energy in external laser field $E(t) = E_0\,cos\,(w_L t)$.

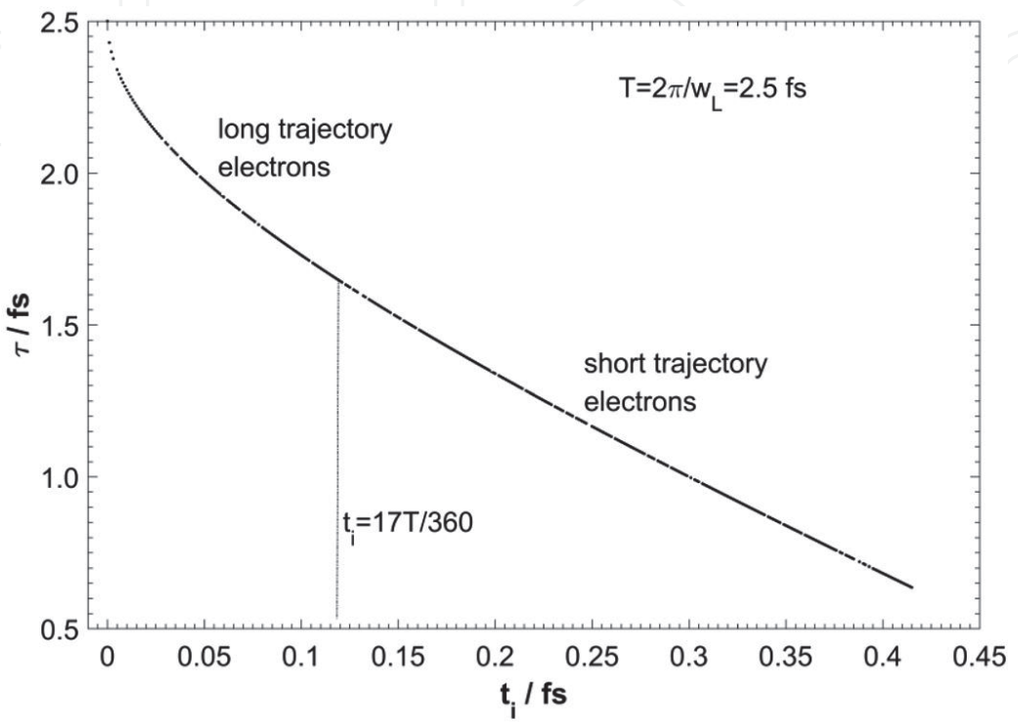

Figure 5.
Electron's free time during the process of HHG.

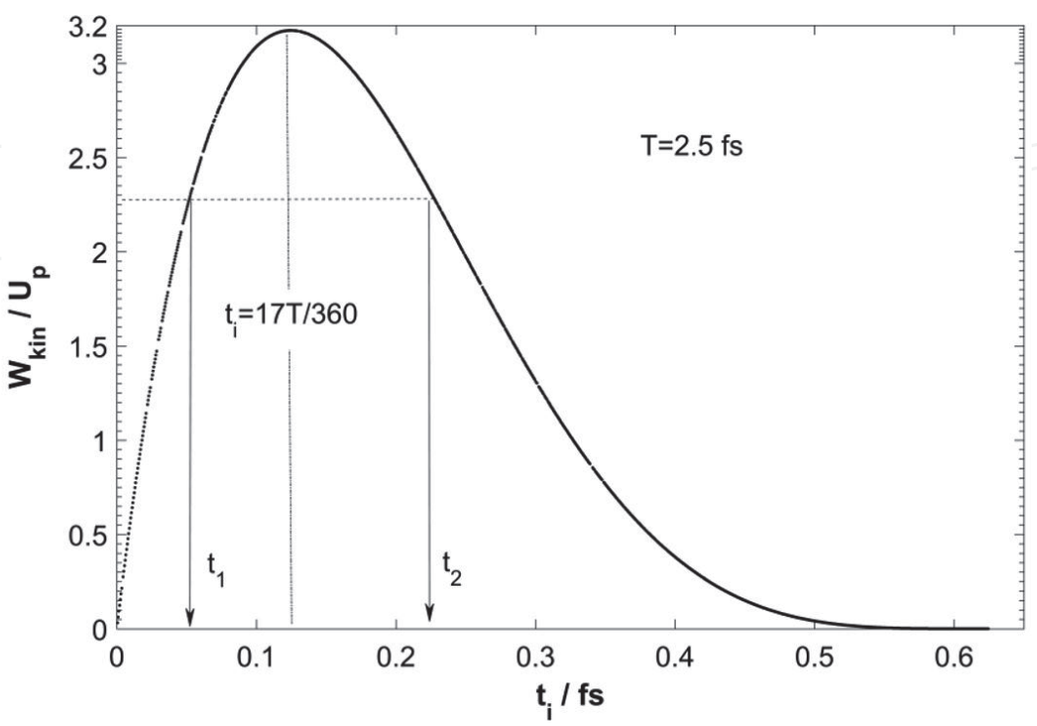

Figure 6.
Electron's return energy during the process of HHG.

The electrons with different freed time t_i are bound to have different free times τ but might have equal return kinetic energy, as shown in **Figures 5** and **6**. Taking the characteristic time $t_m = 17T/360$ as the boundary, which corresponds to the maximum return kinetic energy of 3.17 U_p, electrons freed earlier are called long trajectory electrons, while the others short trajectory electrons. The intrinsic phase of high-order harmonics resulted from the latter definitely has linear chirp, since the parameter τ linearly determining the phase has linear feature.

3. CEP dependence of single attosecond pulse generation

Single isolated attosecond pulses originated from HHG process have been demonstrated experimentally by a variety of gating techniques, which include spectral selection of half-cycle cutoffs as in amplitude gating (AG) [11, 16, 17] and ionization gating (IG) [18–21], temporal gating techniques such as polarization gating (PG) (including double optical gating) [12, 22–27], and spatiotemporal gating with the attosecond lighthouse effect [28, 29]. Based on the intuitive description of HHG as the three-step scenario, PG and AG are the two most fundamental techniques, of which the former utilizes the dependence of HHG yield on driving field ellipticity, while on the latter the essential dependence of HHG itself is on driving field intensity.

PG involves the synthesis of laser field tailored specifically with time-dependent ellipticity. The left and right circularly polarized Gaussian laser fields used are as follows:

$$\vec{E}_{LC}(t) = E_0\left[e^{-2ln\,(2)\frac{(t-T_d/2)^2}{\tau_\omega{}^2}}\right]\left[cos\left(\frac{2\pi}{T}t + CEP\right)\hat{x} + sin\left(\frac{2\pi}{T}t + CEP\right)\hat{y}\right], \quad (6)$$

$$\vec{E}_{RC}(t) = E_0\left[e^{-2ln\,(2)\frac{(t+T_d/2)^2}{\tau_\omega{}^2}}\right]\left[cos\left(\frac{2\pi}{T}t + CEP\right)\hat{x} - sin\left(\frac{2\pi}{T}t + CEP\right)\hat{y}\right]. \quad (7)$$

Here T_d is the time delay between the two laser pulses. So one can get the field synthesized and its ellipticity:

$$\begin{aligned}\vec{E}_C(t) = {} & E_0\left[e^{-2\ln(2)\frac{(t-T_d/2)^2}{\tau_\omega{}^2}} + e^{-2\ln(2)\frac{(t+T_d/2)^2}{\tau_\omega{}^2}}\right] cos\left(\frac{2\pi}{T}t + CEP\right)\hat{x} \\ & + E_0\left[e^{-2\ln(2)\frac{(t-T_d/2)^2}{\tau_\omega{}^2}} - e^{-2\ln(2)\frac{(t+T_d/2)^2}{\tau_\omega{}^2}}\right] sin\left(\frac{2\pi}{T}t + CEP\right)\hat{y}, \quad (8)\end{aligned}$$

$$\xi(t) = \frac{\left|1 - e^{-4\ln(2)\left(T_d/\tau_\omega{}^2\right)t}\right|}{\left|1 + e^{-4\ln(2)(T_d/\tau_\omega{}^2)t}\right|}. \quad (9)$$

The field in Eq. (8) can be decomposed into two linearly polarized fields, the driving field and gating field for HHG, respectively. Taking $\tau_\omega = 2T = 5fs$, $T_d = 5fs$, and the critical field ellipticity $\xi_c = 0.2$ [30], one can have the gating zone with notable HHG effect as $T_G = 1.5fs$. As shown in **Figure 7**, the two channels for HHG are appearing different evolutionary characteristics corresponding to the CEP changing from 0 to $\pi/2$, with channel ① depressed and channel ② enhanced. The intensity contrast between the HHG that resulted reaches the maximum at CEP $= \pi/2$, meaning the generation of single isolated attosecond pulse from one driving laser pulse. Consequently the optimized phase setting for driving field is CEP $= \pi/2$.

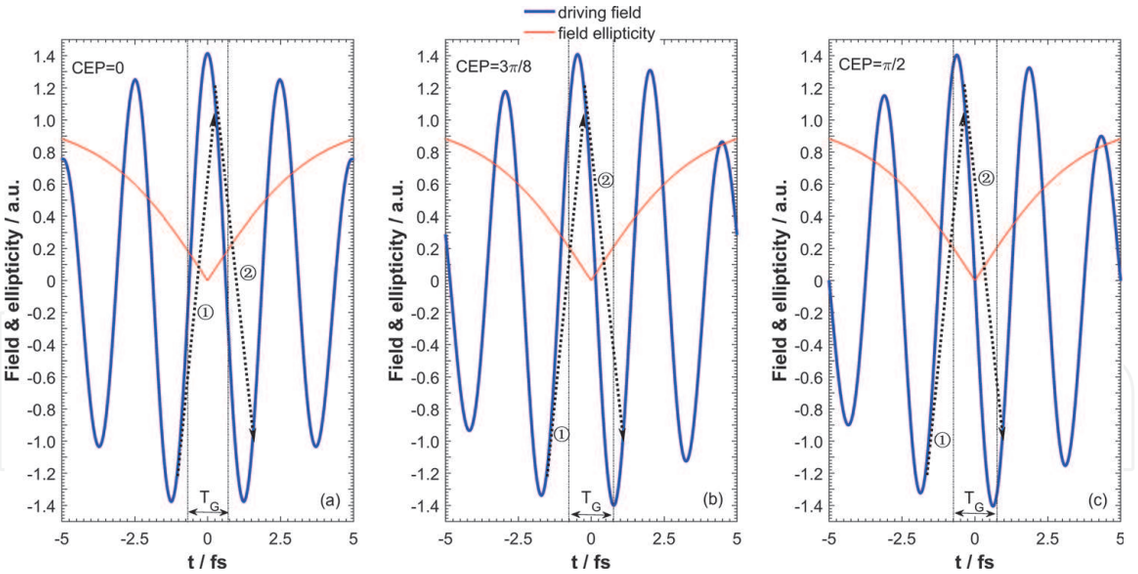

Figure 7.
CEP dependence of HHG for PG.

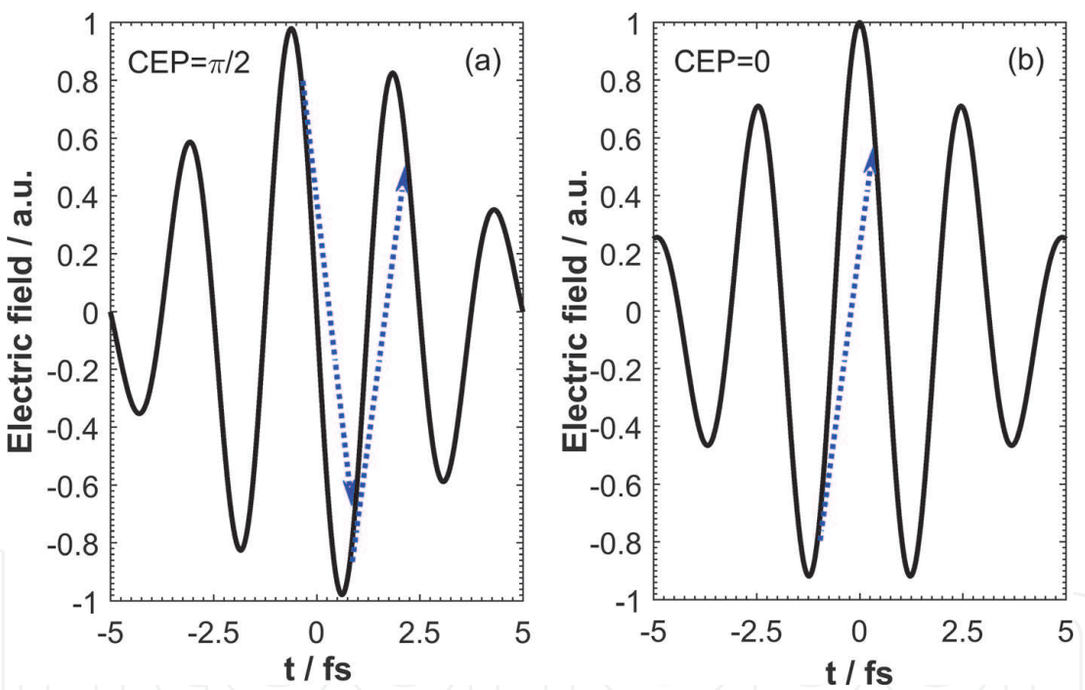

Figure 8.
CEP dependence of HHG for AG.

As for AG, the essence is spectral selection of half-cycle HHG cutoffs, so the linearly polarized driving field with CEP = 0 could guarantee that the cutoff spectrum only comes from one channel and thus is supercontinuum supporting single isolated attosecond pulse, as shown in **Figure 8**. So the optimized phase setting for AG comparatively is CEP = 0, which has been proven by the experimental results in Ref. [16].

4. Phase matching for high-energy attosecond pulse

The device used for optimizing HHG phase matching is schematically shown in **Figure 9**. The CEP stabilized few-cycle femtosecond laser (ladled as 1) is used as the

driving optical field for HHG, with the inert gas (ladled as 5) in the nickel tube (ladled as 4) as the target source. The metal filter (ladled as 8), e.g., aluminum or zirconium, is used to filter the spectrum of residual driving laser from the HHG generated. Acrylic cover (ladled as 12) is specifically adopted for easier monitoring of the driving laser condition when the system is in vacuum. The procedure for optimizing high-order harmonics phase matching includes three steps. The details are deliberated in order as follows.

The first step is done in air. A Ti:sapphire oscillator (Rainbow, Femtolasers GmbH) produces sub-10-fs seed pulses with 2.4-nJ energy at 76-MHz. The oscillator was pumped by a continuous wave laser (Coherent Verdi) at 532-nm and 3.10-watt. The oscillator output pulses are then stretched before coupling them into the amplifier. The output of the nine-pass amplifier with three-mirror configuration was more than 1.1-mJ with hundreds of picosecond duration and 3-kHz repetition rate. After amplification, the beam is sent into a grating compressor consisting of two high-efficiency transmission gratings and a vertical retro-reflector to get 25-fs laser pulse of 0.95-mJ. The beam from this laser system was focused into a fused silica hollow-core fiber filled with neon gas with a length of 1.2-m (250-μm inner diameter and 750-μm outer diameter) [31]. The broad optical spectrum ranging from 420-nm to around 950-nm obtained by self-phase modulation effect in hollow-core fiber, after traveling through a set of finely designed chirped-mirror compressor, gives laser pulse width of 4.6-fs which is about 1.7 optical cycles for the center wavelength of 803.5-nm, as shown in **Figure 10**. With focus spot size of 50-μm, the peak intensity reaches above the level of 1.5×10^{14} W/cm^2, which is enough to initiate the HHG in inert gas. The high-intensity femtosecond laser pulse will bring about air breakdown plasma near its focus, the color of which is blue and purple, as shown in **Figure 11**. Under the dark atmosphere, the longitudinal mid-point of the plasma can be roughly regarded as the focus point of the driving pulse. What is worth mentioning is that, before sending the drive pulse to the vacuum chamber, both the nickel tube and the metal filter plates must not be in the propagation path of the driving pulse.

Subsequent experimental steps are done using the focus point determined as a benchmark. Firstly, keep the driving femtosecond laser in its experimental settings, and roughly place the nickel tube 3 ~ 5-mm after the focus point (yet outside the driving laser path by now to avoid damage). The nickel tube is a hollow-core cylinder with an outer diameter of 2.5-mm and inner diameter of 2.0-mm, the top of which is fully sealed to keep the inert gas system. Secondly, lower the power of the driving laser and then move slowly the nickel tube into the laser path so that the

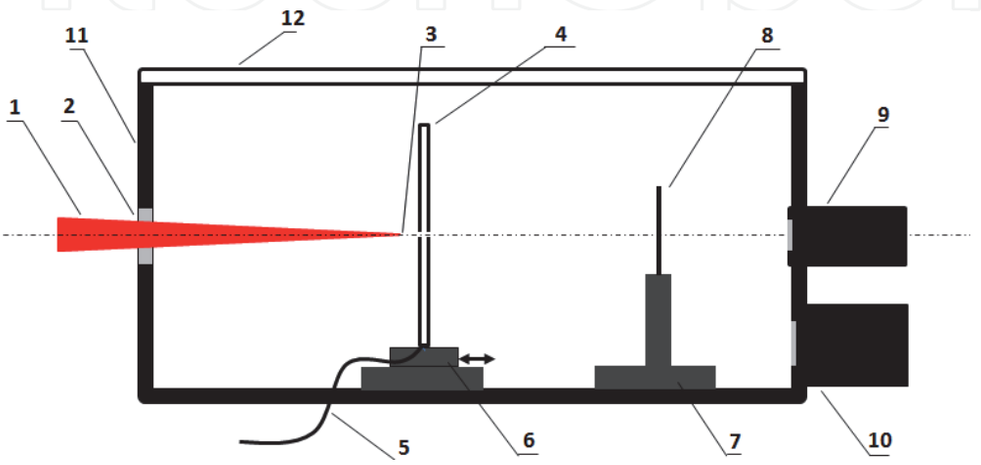

Figure 9.
Schematic diagram of the HHG experimental illustration.

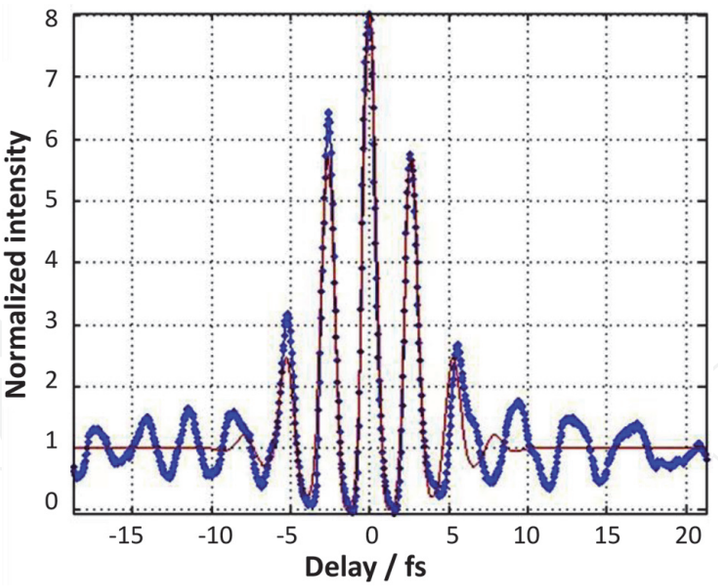

Figure 10.
Autocorrelation trace of laser pulse width measurement.

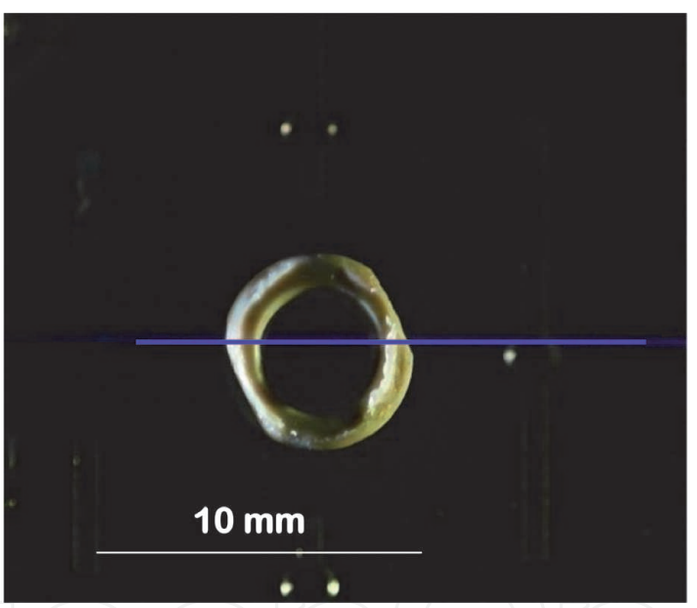

Figure 11.
Strong laser-driven air breakdown plasma.

laser beam spot is just located at the transverse center of the gas tube. At this time the laser power should be too low to make any ablation of the nickel tube. Finally, recover the driving laser power gradually to its experimental value to drill the nickel tube. To reduce the impact of the surrounding air flow on the driving laser beam pointing stability, it is necessary to put the acrylic cover back to get nice tube drilling. It takes at least 30 minutes to finish the drilling process, and the quality can be checked through the pinhole far-field diffraction image, as shown in **Figure 12**.

This part illustrates the details to achieve the optimum phase matching for the most efficient harmonic conversion output. The zirconium filter of thickness of 0.15-μm is used, and its spectral transmittance characteristics are shown in **Figure 13**. When the HHG chamber reaches the required degree of vacuum, 2×10^{-4} Pa or even lower, send the driving femtosecond laser and open the neon gas pipeline control valve to generate high-order harmonics. The high-order

harmonics signal is collected by an X-ray CCD. For the given driving laser settings and nickel tube position, the maximum high-order harmonics yield can be found by finely tuning the backing pressure of the incoming neon gas. By changing the nickel tube position, one can obtain the dependency of high-order harmonics yield on the relative position between the driving laser focus and the target source.

The results are shown in **Figure 14**, in which the horizontal ordinate of 0 indicates the focus point of the driving laser traveling along the positive direction. The optimum phase matching can be arrived when the nickel tube gas target is placed at about 4-mm after the driving laser focus, indicated by the maximum high-order harmonics yield there. The harmonics yield is showing significant asymmetry and is extremely low for the target position before the driving laser focus, which is different from the result of reference [9]. The beam profiles of the high-order harmonics detected by CCD and the driving field at the gas target are shown in **Figures 15** and **16**, respectively. It shows that, under the condition of optimum harmonics phase matching with gas target positioned about 4-mm after the driving laser focus, the harmonics generated have similar intensity spatial distribution with the driving laser field, providing an experimental evidence for the commonly used

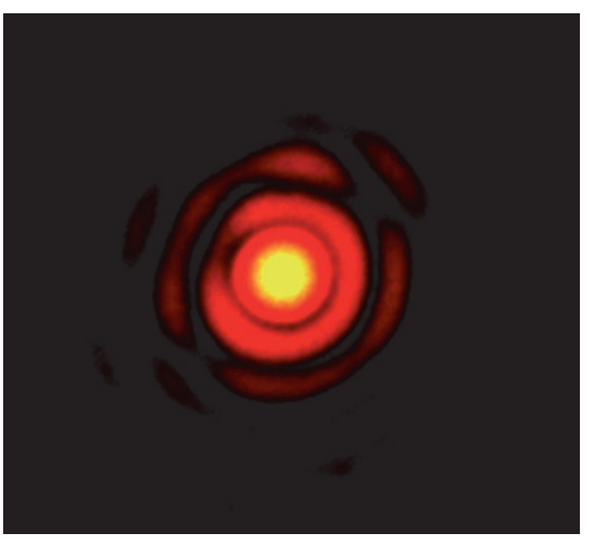

Figure 12.
Far-field pinhole diffraction image of the laser-drilled nickel tube.

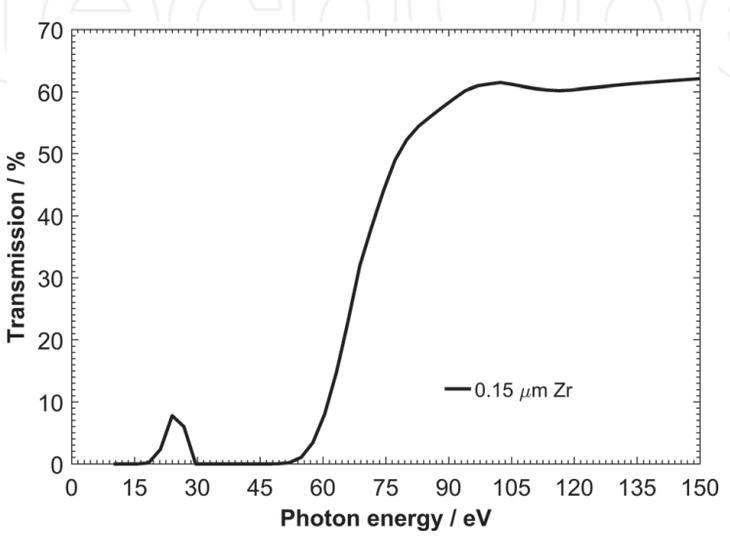

Figure 13.
Transmittance characteristics of 0.15-μm zirconium filter [32].

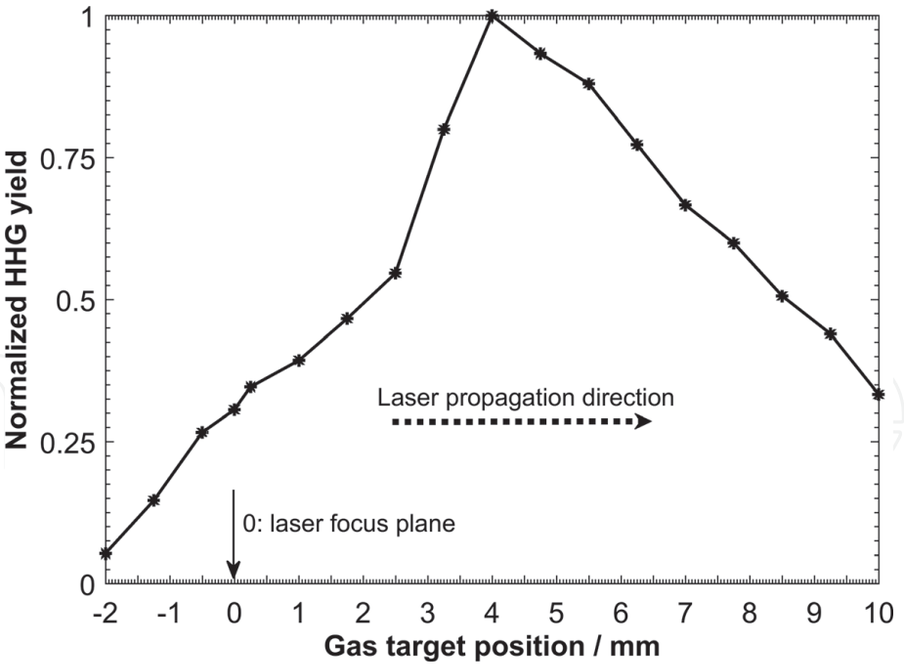

Figure 14.
Dependence of high-order harmonics yield on gas target position.

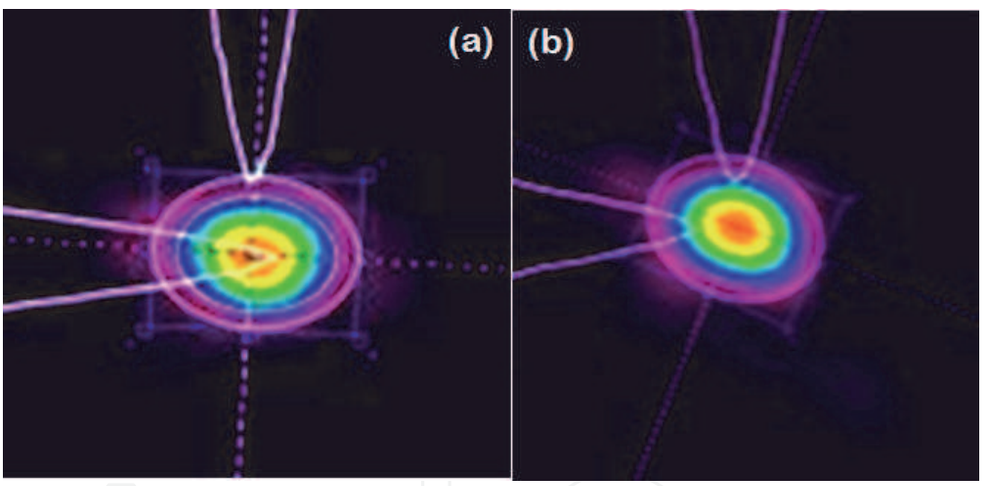

Figure 15.
Driving laser profiles at (a) 4-mm and (b) 2.5-mm after its focus.

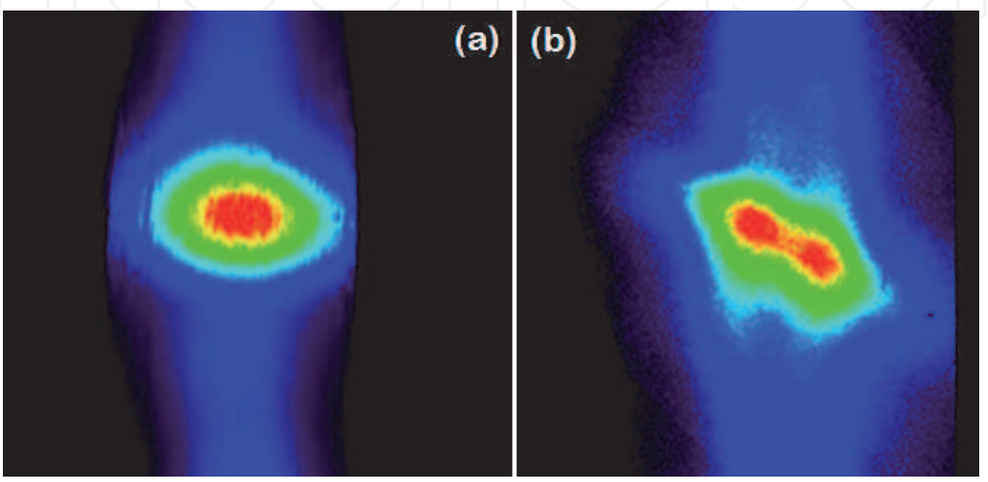

Figure 16.
Far-field profiles of the high-order harmonics with gas target positioned at (a) 4-mm and (b) 2.5-mm after the driving laser focus.

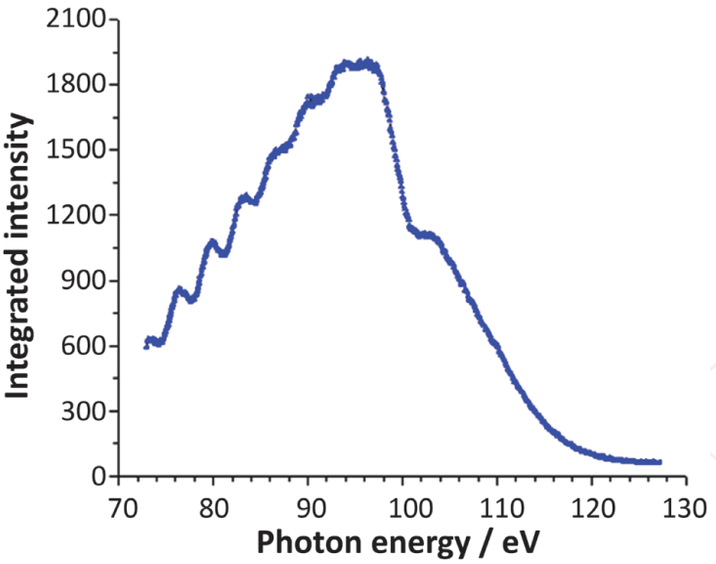

Figure 17.
High-order harmonics spectrum.

assumption that the single isolated attosecond pulse generated by a Gaussian femtosecond laser is also a Gaussian beam. But for the case of worse phase matching as in **Figure 15(b)**, a Gaussian driving laser does not necessarily generate high-order harmonics with similar profile. Using a grazing incidence flat-field spectrometer, the HHG spectrum is analyzed and shown in **Figure 17**. The spectrum in the cutoff region is continuum, indicating that only one channel gave its contribution for the HHG as in **Figure 8(b)**.

It is worth mentioning that other nickel tubes with different inner diameter sizes were also tried. The findings showed that optimum phase matching of HHG existing after the driving laser focus keeps the same for all these experimental situations, though the gas target position for best harmonic phase matching, the harmonics yield, and the backing pressure of gas target used vary to some extent. So we can safely say that the conclusion is universal for Gaussian-type driving laser-based HHG process.

5. Conclusions

The establishment of novel attosecond light source gave rise to an attosecond research upsurge from physics, chemistry, and material science to information processing, among which high-energy single isolated attosecond pulse resulted by interaction between strong optical field and noble gases which has been attracting much attention. Phase matching between the fundamental driving laser field and the high-order harmonics resulted is the key issue to such frequency conversion. In this chapter we scrutinized the intrinsic phase of high-order harmonics resulted from the atom tunneling ionization induced by strong laser field and analyzed qualitatively the salient dependence of polarization gating and amplitude gating on CEP of femtosecond driving laser. The conclusion is that the optimized CEP of driving femtosecond laser for generating single attosecond pulse is $\pi/2$ and 0 for techniques of polarization gating and amplitude gating, respectively. Meanwhile, an implementation was presented experimentally to exemplify the details for optimum HHG phase matching in the interaction of Gaussian-shaped high-intensity few-cycle femtosecond laser with inert gas target. We studied the dependence of the harmonics phase matching on the relative position between the gas target source

and driving laser field focus and found that the optimum gas target position for HHG phase matching is always lying behind the focus of the driving field.

Acknowledgements

The work was supported by the National Natural Science Foundation of China (Grant No. 11675258, 11505289, 61690222).

Author details

Chao Wang[1*], Yifan Kang[2] and Yonglin Bai[1]

1 Key Laboratory of Ultra-fast Photoelectric Diagnostics Technology, Xi'an Institute of Optics and Precision Mechanics, Chinese Academy of Sciences, Xi'an, People's Republic of China

2 School of Science, Air Force Engineering University, Xi'an, People's Republic of China

*Address all correspondence to: igodwang@163.com

References

[1] Wegener M. Extreme Nonlinear Optics. Berlin Heidelberg: Springer-Verlag; 2005. p. 224. DOI: 10.1007/b137953

[2] Nisoli M, De SS, Svelto O, et al. Compression of high-energy laser pulses below 5 fs. Optics Letters. 1997;**22**:522-524. DOI: 10.1364/OL.22.000522

[3] Wegener M. Extreme Nonlinear Optics. 1st ed. Heidelberg: Springer-Verlag Berlin Heidelberg; 2005. p. 223. DOI: 10.1007/b137953

[4] Chang Z. Fundamentals of Attosecond Optics. 1st ed. Florida: CRC Press; 2011. p. 536

[5] Hentschel M, Kienberger R, Ch S, et al. Attosecond metrology. Nature. 2001;**414**:509-513. DOI: 10.1038/35107000

[6] Krausz F, Ivanov M. Attosecond physics. Reviews of Modern Physics. 2009;**81**:163-234. DOI: 10.1103/RevModPhys.81.163

[7] Chang Z, Corkum P. Attosecond photon sources: The first decade and beyond [invited]. Journal of the Optical Society of America B: Optical Physics. 2010;**27**:B9-B17. DOI: 10.1364/JOSAB.27.0000B9

[8] Calegari F, Ayuso D, Trabattoni A, et al. Ultrafast electron dynamics in phenylalanine initiated by attosecond pulses. Science. 2014;**346**:336-339. DOI: 10.1126/science.1254061

[9] Despre V, Marciniak A, Loriot V, et al. Attosecond hole migration in benzene molecules surviving nuclear motion. The Journal of Physical Chemistry Letters. 2015;**6**:426-431. DOI: 10.1021/jz502493j

[10] Hassan M. Attomicroscopy: From femtosecond to attosecond electron microscopy. Journal of Physics B: Atomic, Molecular and Optical Physics. 2018;**51**:1-30. DOI: 10.1088/1361-6455/aaa183

[11] Goulielmakis E, Schultze M, Hofstetter M, et al. Single-cycle nonlinear optics. Science. 2008;**320**:1614-1617. DOI: 10.1126/science.1157846

[12] Sansone G, Benedetti E, Calegari F, et al. Isolated single-cycle attosecond pulses. Science. 2006;**314**:443-446. DOI: 10.1126/science.1132838

[13] Corkum P. Plasma perspective on strong-field multiphoton ionization. Physical Review Letters. 1993;**71**:1994-1997. DOI: 10.1103/PhysRevLett.71.1994

[14] Salieres P, L'Huilier A, Lewenstein M. Coherence control of high-order harmonics. Physical Review Letters. 1995;**74**:3776-3779. DOI: 10.1103/PhysRevLett.74.3776

[15] Gragossian A, Seletskiy DV, Sheik-Bahae M. Classical trajectories in polor-asymmetric laser fields: Synchronous THz and XUV emission. Scientific Reports. 2016;**6**:34973/1-34973/8. DOI: 10.1038/srep34973

[16] Kienberger R, Goulielmakis E, Uiberacker M, et al. Atomic transient recorder. Nature. 2004;**427**:817-821. DOI: 10.1038/nature02277

[17] Witting T, Frank F, Okell WA, et al. Sub-4-fs laser pulse characterization by spatially resolved spectral shearing interferometry and attosecond streaking. Journal of Physics B: Atomic, Molecular and Optical Physics. 2012;**45**:074014/1-074014/6. DOI: 10.1088/0953-4075/45/7/074014

[18] Jullien A, Pfeifer T, Abel MJ, et al. Ionization phase-match gating for wavelength-tunable isolated attosecond pulse generation. Applied Physics B. 2008;**93**:433-442. DOI: 10.1007/s00340-008-3187-z

[19] Abel MJ, Pfeifer T, Nagel PM, et al. Isolated attosecond pulses from ionization gating of high-harmonic emission. Chemical Physics. 2009;**366**: 9-14. DOI: 10.1016/j.chemphys.2009.09.016

[20] Thomann I, Bahabad A, Liu X, et al. Characterizing isolated attosecond pulses from hollow-core waveguides using multi-cycle driving pulses. Optics Express. 2009;**17**:4611-4633. DOI: 10.1364/OE.17.004611

[21] Ferrari F, Calegari F, Lucchini M, et al. High-energy isolated attosecond pulses generated by above-saturation few-cycle fields. Nature Photonics. 2010;**4**:875-879. DOI: 10.1038/nphoton.2010.250

[22] Corkum PB, Burnett NH, Ivanov MY. Subfemtosecond pulses. Optics Letters. 1994;**19**:1870-1872. DOI: 10.1364/OL.19.001870

[23] Sola IJ, Mevel E, Elouga L, et al. Controlling attosecond electron dynamics by phase-stabilized polarization gating. Nature Physics. 2006;**2**:319-322. DOI: 10.1038/nphys281

[24] Zhao K, Zhang Q, Chini M, et al. Tailoring a 67 attosecond pulse through advantageous phase-mismatch. Optics Letters. 2012;**37**:3891-3893. DOI: 10.1364/OL.37.003891

[25] Mashiko H, Gilbertson S, Li C, et al. Double optical gating of high-order harmonic generation with carrier-envelope phase stabilized lasers. Physical Review Letters. 2008;**100**: 103906/1-103906/4. DOI: 10.1103/PhysRevLett.100.103906

[26] Feng X, Gilbertson S, Mashiko H, et al. Generation of isolated attosecond pulses with 20 to 28 femtosecond lasers. Physical Review Letters. 2009;**103**: 183901/1-183901/4. DOI: 10.1103/PhysRevLett.103.183901

[27] Mashiko H, Bell MJ, Beck AR, et al. Tunable frequency-controlled isolated attosecond pulses characterized by either 750 nm or 400 nm wavelength streak fields. Optics Express. 2010;**18**: 25887-25895. DOI: 10.1364/QELS.2011.QMG4

[28] Vincenti H, Quéré F. Attosecond lighthouses: How to use spatiotemporally coupled light fields to generate isolated attosecond pulses. Physical Review Letters. 2012;**108**: 113904/1-113904/5. DOI: 10.1103/PhysRevLett.108.113904

[29] Kim KT, Zhang C, Ruchou T, et al. Photonic streaking of attosecond pulse trains. Nature Photonics. 2013;**7**: 651-656. DOI: 10.1038/NPHOTON.2013.170

[30] Antoine P, L'Huillier A, Lewenstein M, et al. Theory of high-order harmonic generation by an elliptically polarized laser field. Physical Review A. 1996;**53**:1725-1745. DOI: 10.1103/PhysRevA.53.1725

[31] An J, Kim DE. Compact in-line autocorrelator using double wedge. Optics Express. 2012;**20**:3325-3330. DOI: 10.1364/OE.20.003325

[32] Available at: http://henke.lbl.gov/optical_constants/filter2.html [Accessed: 20 May 2018]